Table 2 Evaluation of risk for recurrence and progression using univariate analysis

	Total cases		Recurrence/progression	Non-recurrence/progression	*p* value
Cases	37		8	29	
Age (years)	37		57.9 ± 11.8	53.6 ± 13.2	0.41
Gender	37	Female	3	20	
		Male	5	9	0.22
Skull base	37	Yes	5	11	
		No	3	18	0.25
LN ratio	37		3.67 ± 1.15	2.65 ± 0.86	<0.01
Extent of resection	33	GTR	1	17	
		Non-GTR	5	10	0.053
WHO grade	33	Grade I	5	25	
		Grade II	1	2	0.46
Ki-67 LI	33		1.81 ± 1.21	3.06 ± 3.84	0.44

The LN ratio was a significant risk factor for recurrence and progression

LN lesion to normal, *GTR* gross total resection, *LI* labeling index

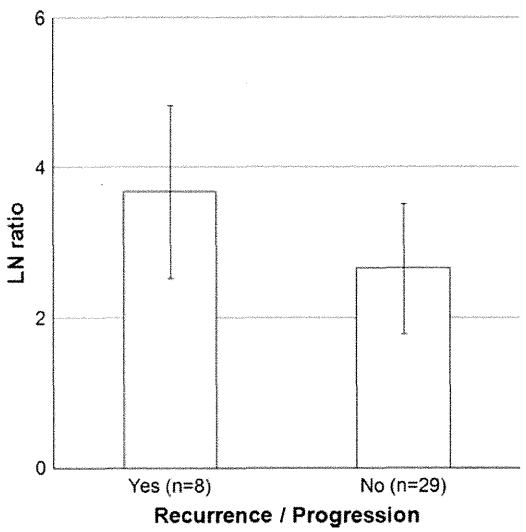

Fig. 2 LN ratio of MET PET and recurrence/progression. The LN ratio in cases with recurrence and progression was significantly higher than that in cases without recurrence and progression ($p < 0.01$)

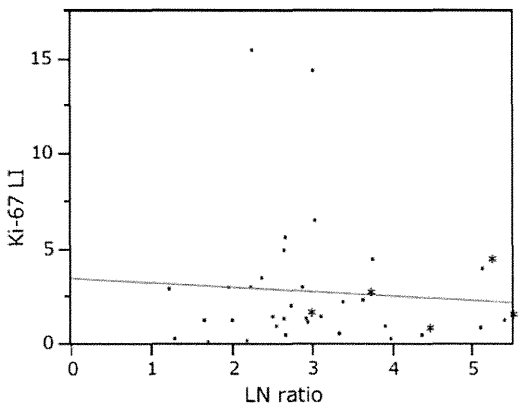

Fig. 3 Correlation between the LN ratio of MET PET and the Ki-67 LI. No correlation between the LN ratio and the Ki-67 LI was observed. *Asterisks* cases with recurrence or progression

level of the LN ratio for predicting recurrence and progression. ROC analysis confirmed 3.18 as the best predictive cutoff value of the LN ratio for recurrence and progression. The AUC was 0.754. Using the best cutoff value of 3.18, the sensitivity and specificity were 63 and 79 %, respectively (Fig. 5).

Discussion

The risk factors for recurrence and progression in meningioma have been reported in many previous studies. They include age [5, 6], gender [7], tumor size [8], calcification [7, 9], brain invasion [10], location [11], vascular density [12], Ki-67 LI [8, 13–15], extent of the resection [12, 16, 17], and WHO grade [11]. In our study, age, gender, tumor location, Ki-67 LI, and the LN ratio of MET PET were investigated. A high LN ratio was significantly correlated with tumor recurrence and progression. However, age, gender, tumor location, and KI-67 LI were not significantly correlated with tumor recurrence. These risk factors remain controversial.

Recently, the MET PET method has been used in gliomas and other intracranial tumors to evaluate the malignancy of the tumor and the proliferative activity. In previous studies of gliomas, MET uptake correlated with the WHO grade, Ki-67 LI, and patient survival [18–21]. However, the role of MET PET in meningioma is not clear. In a previous study using ^{18}F-fluorodeoxyglucose (FDG) PET, ^{18}F-FDG uptake was correlated with the Ki-67 LI but not with recurrence of the meningioma [22, 23]. Using

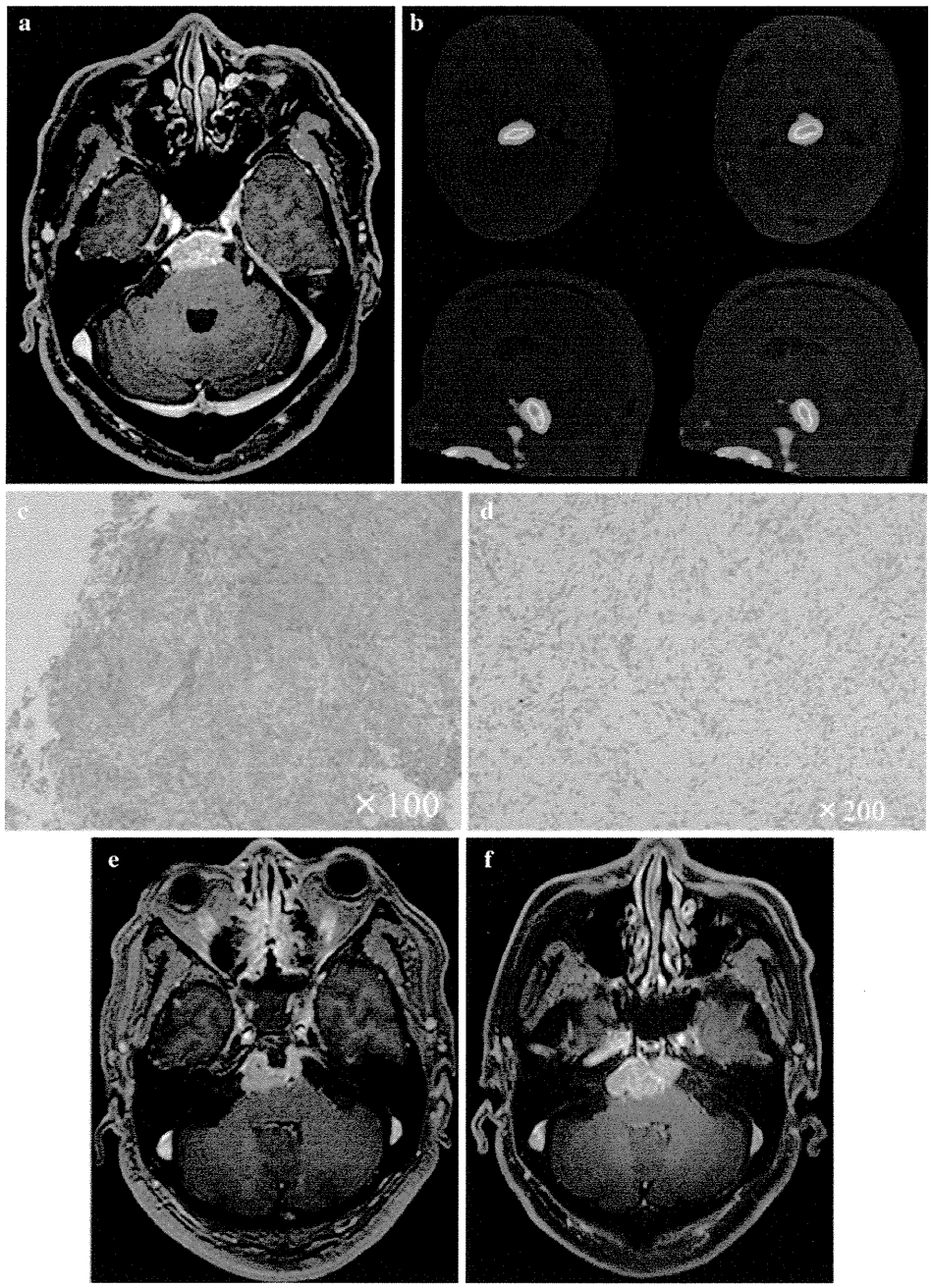

Fig. 4 Case 36. **a** Preoperative Gadolinium (Gd)-enhanced T1-weighted image. The tumor is located at the clivus. **b** ^{11}C-methionine was taken up into the tumor. The LN ratio was 4.35. **c**, **d** Photomicrograph of a sample of the lesion. Hematoxylin and eosin-stained section (**c** ×100) and Ki-67 staining (**d** ×200) of a meningioma tissue specimen. The diagnosis based on pathology was meningothelial meningioma. The Ki-67 LI was 0.5. **e** Postoperative Gd-enhanced T1-weighted image. In this case, the tumor was partially removed using a trans-sphenoidal approach. **f** Gd-enhanced T1-weighted image 15 months after surgery. The tumor had begun to grow again

kinetic analysis with ^{18}F-FDG PET, Tsuyuguchi [24] showed that the kinetic rate constant of glucose metabolism is related to the Ki-67 LI. However, that analysis requires frequent arterial blood samplings and dynamic PET scanning. The procedure is very complicated and not practical for clinical use. Moreover, the results of ^{18}F-FDG PET are influenced by blood glucose. In patients with hyperglycemia, the results may lead to overestimation [25]. Iuchi et al. [26] showed that MET uptake is significantly correlated with the count of nuclear organizer regions, which is a histological index of protein synthesis, the Ki-67 LI, and a histological index of proliferative activity. In that study,

^{18}F-FDG uptake showed no significant correlation with the Ki-67 LI or clinical malignancy. The uptake of methionine reflects amino acid transport and metabolism, but this does not mean that methionine uptake is correlated with protein synthesis and proliferation [27]. Some previous studies have shown that MET uptake correlates with microvessel density in glioma cases [28, 29], but in meningioma cases, MET uptake does not correlate with microvessel density [30]. This observation may reflect the fact that meningioma has multiple pathological subtypes and, thus, microvessel density may be different in each subtype. To evaluate the correlation between the LN ratio and microvessel density in meningioma, many cases of each subtype would be necessary.

Arita et al. [30] showed that the LN ratio of MET uptake is not significantly correlated with tumor doubling time. In this study, many asymptomatic patients were enrolled, and the mean tumor doubling time was very long (174 ± 270 months) despite a short follow-up period (26.7 ± 16.7 months). Thus, evaluation of recurrence and progression in meningioma using tumor doubling time appeared to be difficult because most meningiomas progress slowly.

Compared with ^{18}F-FDG PET, the contrast between a meningioma lesion and normal brain tissue is clear in MET PET and, thus, we can correctly define the ROI using MET PET. Recently, we have evaluated MET uptake more correctly by fusing PET images with computed tomography or MR images.

In this study, we calculated the LN ratio using the mean MET uptake of the lesion and the normal brain tissue. The methionine uptake in the tumor depends not only on the metabolic rate, but also on the vascular bed [31]. The vascular bed of the meningioma is different within the various pathological types of meningiomas [32], and the vascular bed may be variable in the same specimen. Biological activity is heterogeneous in the same meningioma lesion [33, 34]. Thus, partially high MET uptake does not always indicate a high metabolic rate of the whole tumor. In this study, we used the mean MET uptake, not the maximum MET uptake, to reduce the influence on the heterogeneity of MET uptake.

Table 3 Evaluation of risk factors for recurrence using Cox proportional hazards model

	p value	Risk ratio
Age (years)	0.28	
Gender	0.43	
Skull base	0.12	
LN ratio	0.03	4.21
Extent of resection (non-GTR/GTR)	0.014	
WHO grade (grade II/grade I)	0.0074	
Ki-67 LI	0.079	

LN ratio, extent of resection, and WHO grade were significant risk factors

LN lesion to normal, *WHO* World Health Organization, *GTR* gross total resection, *LI* labeling index

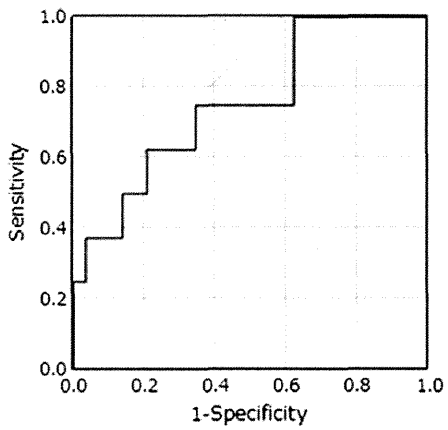

Fig. 5 ROC curve of the LN ratio. AUC of the LN ratio of MET PET was 0.754. The optimal cutoff value was 3.18. The sensitivity and specificity were 63 and 79 %, respectively

Table 4 Evaluation of risk factors for recurrence and progression excluding gross total resection cases

	Total cases		Recurrence/progression	Non-recurrence/progression	*p* value
Cases	19		7	12	
Age (years)	19		58.6 ± 12.5	57.8 ± 13.2	0.9
Gender	19	Female	2	7	
		Male	5	5	0.35
Skull base	19	Yes	5	6	
		No	2	6	0.63
LN ratio	19		3.84 ± 1.13	2.74 ± 1.02	0.04
Surgical cases			5	10	
WHO grade	15	Grade I	5	10	
		Grade II	0	0	
Ki-67 LI	15		1.87 ± 1.35	1.06 ± 0.87	0.18

Only the LN ratio was significantly different between the recurrence/progression group and the non-recurrence/progression group

LN lesion to normal, *WHO* World Health Organization, *LI* labeling index

In this study, tumor progression and recurrence were not significantly different between the GTR and non-GTR groups. However, in some cases with a high Ki-67 LI, GTR was performed, and the recurrence rate was low. GTR was a factor that strongly influenced the recurrence rate. We evaluated the recurrence and progression in the non-GTR group. The LN ratio in the group with recurrence and progression was also significantly higher than that in the group without recurrence and progression ($p < 0.05$). The Ki-67 LI was not significantly different ($p = 0.18$). Our observations are summarized in Table 4.

In our study, the LN ratio was a significant risk factor for recurrence and progression. The LN ratio of MET PET may indicate the proliferative activity of meningioma. Using ROC analysis, the AUC was 0.754, and the best cutoff value was 3.18, resulting in a sensitivity and specificity of 63 and 79 %, respectively. The sensitivity and specificity of the LN ratio were not less than those of the Ki-67 LI, as described in a previous study [35, 36].

In our study, the Ki-67 LI was not significantly different between the patients with recurrence and those without. We also found no correlation between the LN ratio and the Ki-67 LI. Some previous papers have reported that the correlation between the Ki-67 LI and tumor recurrence is controversial [4, 33, 37, 38]. Meningioma is characterized by heterogeneous biological activity within the same tumor tissue [33, 34]. It is doubtful that the Ki-67 LI obtained from a small tumor specimen can adequately evaluate the proliferative potential of the whole tumor. In fact, MET uptake is heterogeneous in a large tumor and may reflect the heterogeneity of the Ki-67 LI. The MET PET method is useful for evaluating the whole tumor. The Ki-67 LI overlaps within each grade of meningioma [39–41]. Evaluating the proliferative activity of the whole tumor and providing an accurate prognosis may be difficult with only one index.

The extent of resection was a significant risk factor as shown in a previous study [12, 16, 17]. However, the location of the tumor was not a significant risk factor in this study. Sixteen cases of skull base meningioma were included. In these cases, total resection without complications is difficult. A GTR of the tumor would reduce the risk of recurrence. This result may indicate that additional treatments are necessary for a residual tumor in which the LN ratio is higher than 3.18.

The WHO grade of meningioma was also a significant risk factor. In this study, we investigated preoperative cases and, thus, most cases were WHO grade I; only three cases were WHO grade II. Cases with WHO grade III meningioma are relatively infrequent at initial diagnosis. Almost all cases of meningioma are pathologically benign. Thus, we have to follow patients for a long time to investigate malignant changes and the prognosis. We must investigate additional consecutive cases to evaluate the largest number and the widest variety of cases.

Our study showed that the MET PET method has useful sensitivity and specificity for evaluation of recurrence and progression in meningioma. The most beneficial point is that ^{11}C-methionine PET is not invasive, whereas analysis of the Ki-67 LI requires surgery. Thus, without surgery, we can evaluate the risk of progression and recurrence and consider the treatment strategy. We can determine the risk of progression and recurrence before deciding on observation or surgery. In asymptomatic cases, high LN ratio of MET PET may be the decisive factor for determining surgical treatment. We did not evaluate a large number of cases, and thus continued collection of cases and evaluation of the data are necessary.

Conclusion

The results of our study showed that MET uptake by the meningioma was a significant prognostic factor. MET uptake was significantly higher in cases with recurrence or progression. The AUC of the LN ratio for recurrence or progression was 0.754, and the best cutoff value was 3.18. The greatest advantage associated with the MET PET method is its non-invasive nature.

Acknowledgments The authors appreciate the technical support of the radiological technologist at our institute.

Conflict of interest The authors have no personal financial or institutional interest in any of the drugs, materials, or devices described in this article.

References

1. Committee of Brain Tumor Registry of Japan. Report of Brain Tumor Registry of Japan (1984-2000) Neurol Med Chir. 2009;49 Suppl.
2. Crompton MR, Gautier-Smith PC. The prediction of recurrence in meningiomas. J Neurol Neurosurg Psychiatry. 1970;33(1): 80–7.
3. Jellinger K, Slowik F. Histological subtypes and prognostic problems in meningiomas. J Neurol. 1975;208(4):279–98.
4. Roser F, Samii M, Ostertag H, Bellinzona M. The Ki-67 proliferation antigen in meningiomas. Experience in 600 cases. Acta Neurochir. 2004;146(1):37–44 (discussion).
5. McCarthy BJ, Davis FG, Freels S, Surawicz TS, Damek DM, Grutsch J, et al. Factors associated with survival in patients with meningioma. J Neurosurg. 1998;88(5):831–9.
6. Nakamura M, Roser F, Michel J, Jacobs C, Samii M. The natural history of incidental meningiomas. Neurosurgery. 2003;53(1):62–70 (discussion-1).
7. Niiro M, Yatsushiro K, Nakamura K, Kawahara Y, Kuratsu J. Natural history of elderly patients with asymptomatic meningiomas. J Neurol Neurosurg Psychiatry. 2000;68(1):25–8.

8. Kasuya H, Kubo O, Tanaka M, Amano K, Kato K, Hori T. Clinical and radiological features related to the growth potential of meningioma. Neurosurg Rev. 2006;29(4):293–6 discussion 296-297.
9. Kuratsu J, Kochi M, Ushio Y. Incidence and clinical features of asymptomatic meningiomas. J Neurosurg. 2000;92(5):766–70.
10. Alvernia JE, Dang ND, Sindou MP. Convexity meningiomas: study of recurrence factors with special emphasis on the cleavage plane in a series of 100 consecutive patients. J Neurosurg. 2011;115(3):491–8.
11. McGovern SL, Aldape KD, Munsell MF, Mahajan A, DeMonte F, Woo SY. A comparison of World Health Organization tumor grades at recurrence in patients with non-skull base and skull base meningiomas. J Neurosurg. 2010;112(5):925–33.
12. Guevara P, Escobar-Arriaga E, Saavedra-Perez D, Martinez-Rumayor A, Flores-Estrada D, Rembao D, et al. Angiogenesis and expression of estrogen and progesterone receptors as predictive factors for recurrence of meningioma. J Neurooncol. 2010;98(3):379–84.
13. Matsuno A, Fujimaki T, Sasaki T, Nagashima T, Ide T, Asai A, et al. Clinical and histopathological analysis of proliferative potentials of recurrent and non-recurrent meningiomas. Acta Neuropathol. 1996;91(5):504–10.
14. Takeuchi H, Kubota T, Kabuto M, Kitai R, Nozaki J, Yamashita J. Prediction of recurrence in histologically benign meningiomas: proliferating cell nuclear antigen and Ki-67 immunohistochemical study. Surg Neurol. 1997;48(5):501–6.
15. Lanzafame S, Torrisi A, Barbagallo G, Emmanuele C, Alberio N, Albanese V. Correlation between histological grade, MIB-1, p53, and recurrence in 69 completely resected primary intracranial meningiomas with a 6 year mean follow-up. Pathol Res Pract. 2000;196(7):483–8.
16. Adegbite AB, Khan MI, Paine KW, Tan LK. The recurrence of intracranial meningiomas after surgical treatment. J Neurosurg. 1983;58(1):51–6.
17. Mirimanoff RO, Dosoretz DE, Linggood RM, Ojemann RG, Martuza RL. Meningioma: analysis of recurrence and progression following neurosurgical resection. J Neurosurg. 1985;62(1):18–24.
18. Ribom D, Eriksson A, Hartman M, Engler H, Nilsson A, Langstrom B, et al. Positron emission tomography (11)C-methionine and survival in patients with low-grade gliomas. Cancer. 2001;92(6):1541–9.
19. Torii K, Tsuyuguchi N, Kawabe J, Sunada I, Hara M, Shiomi S. Correlation of amino-acid uptake using methionine PET and histological classifications in various gliomas. Ann Nucl Med. 2005;19(8):677–83.
20. Kim S, Chung JK, Im SH, Jeong JM, Lee DS, Kim DG, et al. 11C-methionine PET as a prognostic marker in patients with glioma: comparison with 18F-FDG PET. Eur J Nucl Med Mol Imaging. 2005;32(1):52–9.
21. Kato T, Shinoda J, Oka N, Miwa K, Nakayama N, Yano H, et al. Analysis of 11C-methionine uptake in low-grade gliomas and correlation with proliferative activity. AJNR Am J Neuroradiol. 2008;29(10):1867–71.
22. Lee JW, Kang KW, Park SH, Lee SM, Paeng JC, Chung JK, et al. 18F-FDG PET in the assessment of tumor grade and prediction of tumor recurrence in intracranial meningioma. Eur J Nucl Med Mol Imaging. 2009;36(10):1574–82.
23. Lippitz B, Cremerius U, Mayfrank L, Bertalanffy H, Raoofi R, Weis J, et al. PET-study of intracranial meningiomas: correlation with histopathology, cellularity and proliferation rate. Acta Neurochirurgica Suppl. 1996;65:108–11.
24. Tsuyuguchi N. Kinetic analysis of glucose metabolism by FDG-PET versus proliferation index of Ki-67 in meningiomas–comparison with gliomas. Osaka City Med J. 1997;43(2):209–23.
25. Cremerius U, Bares R, Weis J, Sabri O, Mull M, Schroder JM, et al. Fasting improves discrimination of grade 1 and atypical or malignant meningioma in FDG-PET. J Nucl Med. 1997;38(1):26–30.
26. Iuchi T, Iwadate Y, Namba H, Osato K, Saeki N, Yamaura A, et al. Glucose and methionine uptake and proliferative activity in meningiomas. Neurol Res. 1999;21(7):640–4.
27. Gudjonsson O, Blomquist E, Lilja A, Ericson H, Bergstrom M, Nyberg G. Evaluation of the effect of high-energy proton irradiation treatment on meningiomas by means of 11C-L-methionine PET. Eur J Nucl Med. 2000;27(12):1793–9.
28. Okubo S, Zhen HN, Kawai N, Nishiyama Y, Haba R, Tamiya T. Correlation of L-methyl-11C-methionine (MET) uptake with L-type amino acid transporter 1 in human gliomas. J Neurooncol. 2010;99(2):217–25.
29. Kracht LW, Friese M, Herholz K, Schroeder R, Bauer B, Jacobs A, et al. Methyl-[11C]- L-methionine uptake as measured by positron emission tomography correlates to microvessel density in patients with glioma. Eur J Nucl Med Mol Imaging. 2003;30(6):868–73.
30. Arita H, Kinoshita M, Okita Y, Hirayama R, Watabe T, Ishohashi K, et al. Clinical characteristics of meningiomas assessed by ^{11}C-methionine and ^{18}F-fluorodeoxyglucose positron-emission tomography. J Neurooncol. 2012;107(2):379–86.
31. Abe Y, Matsuzawa T, Itoh M, Ishiwata K, Fujiwara T, Sato T, et al. Regional coupling of blood flow and methionine uptake in an experimental tumor assessed with autoradiography. Eur J Nucl Med. 1988;14(7–8):388–92.
32. Kimura H, Takeuchi H, Koshimoto Y, Arishima H, Uematsu H, Kawamura Y, et al. Perfusion imaging of meningioma by using continuous arterial spin-labeling: comparison with dynamic susceptibility-weighted contrast-enhanced MR images and histopathologic features. AJNR Am J Neuroradiol. 2006;27(1):85–93.
33. Siegers HP, Zuber P, Hamou MF, van Melle GD, de Tribolet N. The implications of the heterogeneous distribution of Ki-67 labelled cells in meningiomas. Br J Neurosurg. 1989;3(1):101–7.
34. Abramovich CM, Prayson RA. Histopathologic features and MIB-1 labeling indices in recurrent and nonrecurrent meningiomas. Arch Pathol Lab Med. 1999;123(9):793–800.
35. Bruna J, Brell M, Ferrer I, Gimenez-Bonafe P, Tortosa A. Ki-67 proliferative index predicts clinical outcome in patients with atypical or anaplastic meningioma. Neuropathology. 2007;27(2):114–20.
36. Kim YJ, Ketter R, Henn W, Zang KD, Steudel WI, Feiden W. Histopathologic indicators of recurrence in meningiomas: correlation with clinical and genetic parameters. Virchows Archiv. 2006;449(5):529–38.
37. Moller ML, Braendstrup O. No prediction of recurrence of meningiomas by PCNA and Ki-67 immunohistochemistry. J Neurooncol. 1997;34(3):241–6.
38. Nakaguchi H, Fujimaki T, Matsuno A, Matsuura R, Asai A, Suzuki I, et al. Postoperative residual tumor growth of meningioma can be predicted by MIB-1 immunohistochemistry. Cancer. 1999;85(10):2249–54.
39. Abramovich CM, Prayson RA. MIB-1 labeling indices in benign, aggressive, and malignant meningiomas: a study of 90 tumors. Hum Pathol. 1998;29(12):1420–7.
40. Kolles H, Niedermayer I, Schmitt C, Henn W, Feld R, Steudel WI, et al. Triple approach for diagnosis and grading of meningiomas: histology, morphometry of Ki-67/Feulgen stainings, and cytogenetics. Acta Neurochir. 1995;137(3–4):174–81.
41. Langford LA, Cooksley CS, DeMonte F. Comparison of MIB-1 (Ki-67) antigen and bromodeoxyuridine proliferation indices in meningiomas. Hum Pathol. 1996;27(4):350–4.

J Neurosurg 120:1–11, 2014

Surgical outcomes of the minimum anterior and posterior combined transpetrosal approach for resection of retrochiasmatic craniopharyngiomas with complicated conditions

Clinical article

Noritsugu Kunihiro, M.D., Takeo Goto, M.D., Kenichi Ishibashi, M.D., and Kenji Ohata, M.D.

Department of Neurosurgery, Osaka City University Graduate School of Medicine, Osaka, Japan

Object. Retrochiasmatic craniopharyngiomas are surgically challenging tumors. Retrochiasmatic craniopharyngiomas with complicated conditions such as large diameter, major calcification, or significant extension to the third ventricle or posterior fossa present surgical challenges; moreover, recurrent retrochiasmatic craniopharyngiomas are particularly formidable challenges. Although the transpetrosal approach to retrochiasmatic craniopharyngiomas published by Hakuba in 1985 can provide unique advantageous exposure of the retrochiasmatic area to allow safe neurovascular dissection and facilitate radical tumor removal, the procedure is viewed as complicated and time consuming and has a high risk of damaging hearing functions. The authors have modified Hakuba's technique to minimize petrosectomy and reduce surgical complications and have applied this modified approach to retrochiasmatic craniopharyngiomas with complicated conditions. In this study, the authors describe their technique and surgical outcomes to elucidate the role of this modified transpetrosal approach for retrochiasmatic craniopharyngiomas with complicated conditions. This is the first study to report surgical outcomes of the transpetrosal approach for retrochiasmatic craniopharyngiomas.

Methods. Between 1999 and 2011, the minimum anterior and posterior combined (MAPC) transpetrosal approach, which is a modification of Hakuba's transpetrosal approach, was applied in 16 cases of retrochiasmatic craniopharyngiomas with complicated conditions. Eight cases were recurrent tumors, 4 had previously received radiotherapy, 11 had a large diameter, 10 had large calcification, 15 had superior extension of the tumor into the third ventricle, and 10 had a posterior extension of the tumor that compressed the midbrain and pons. In all 16 patients, more than 2 of these complicated conditions were present. The follow-up duration ranged from 0.8 to 12.5 years (mean 5.3 years). Surgical outcomes assessed were the extent of resection, surgical complications, visual function, endocrinological status, and neuropsychological function. Five-year and 10-year recurrence-free survival rates were also calculated.

Results. Gross-total or near-total resection was achieved in 15 cases (93.8%). Facial nerve function was completely maintained in all 16 patients. Serviceable hearing was preserved in 15 cases (93.8%). Visual function improved in 13 out of 14 cases (92.9%) that had visual disturbance before surgery. None of the patients experienced deterioration of their visual function. Twelve cases had endocrinological deficit and received hormonal replacement before surgery. New endocrinological deficit occurred in 2 cases (12.5%). Neuropsychological function was maintained in 14 cases (87.5%) and improved in 1 case (6.3%). One case that had received previous conventional radiotherapy treatment showed a gradual decline in neuropsychological function. The 5-year and 10-year recurrence-free survival rates were both 86.5%.

Conclusions. The authors obtained good results by using the MAPC transpetrosal approach for the removal of retrochiasmatic craniopharyngiomas with complicated conditions. The MAPC transpetrosal approach should be considered as a therapeutic option for selected cases of retrochiasmatic craniopharyngiomas with complicated conditions.

(http://thejns.org/doi/abs/10.3171/2013.10.JNS13673)

Key Words • **retrochiasmatic craniopharyngioma** • **skull base** • **surgical approach** • **transpetrosal approach** • **oncology**

Craniopharyngiomas located in retrochiasmatic regions are regarded as particularly challenging tumors to remove safely and totally because of their anatomical location and proximity to critical neurovascular structures.[2,6,26] Surgical resection of this type of craniopharyngioma is associated with high rates of surgical mortality, surgical complications, and incomplete resection resulting in a high recurrence rate.[6,26] Although various surgical approaches to remove retrochiasmatic craniopharyngiomas have been described, including pterional, orbitopterional, orbitozygomatic, transbasal subfrontal, frontobasal interhemispheric, and transnasal transsphenoi-

Abbreviations used in this paper: KPS = Karnofsky Performance Scale; MAPC = minimum anterior and posterior combined; PCoA = posterior communicating artery; VIS = visual impairment scale

dal approaches,[3,5,6,8,10,15–17,22,23,26,29] the optimal surgical approach remains controversial.

In 1985, Hakuba reported the usefulness of the transpetrosal approach for the removal of retrochiasmatic craniopharyngiomas,[11] emphasizing that this approach offers wide exposure of retrochiasmatic lesions and unique posterior-to-anterior and inferior-to-superior projection to the inferior and posterior surfaces of the chiasm, the floor of third ventricle, and the hypothalamic tuber cerium area. However, in his approach, Hakuba sacrificed 3 semicircular canals with 33% hearing preservation. Al-Mefty et al. used Hakuba's techniques and reported the effectiveness of the transpetrosal approach for giant retrochiasmatic craniopharyngiomas[1] but have not yet reported outcomes and complication rates in their surgical series. In addition, the complicated surgical procedures involved in the petrosal approach have discouraged neurosurgeons from assessing the most effective approach for removal of retrochiasmatic craniopharyngiomas.

We have modified Hakuba's techniques to minimize petrosectomy and reduce surgical complications and have applied this approach to 16 patients with retrochiasmatic craniopharyngiomas with complicated conditions such as a history of excision or radiotherapy, tumors with large calcification, large diameter (> 30 mm), superior extension into the third ventricle, or severe posterior extension compressing the midbrain and pons. This study retrospectively analyzed surgical outcomes, including the extent of tumor resection, recurrence rate, surgical complications, visual function, endocrinological status, neuropsychological function, and functional performance status, to elucidate the role of our modified transpetrosal approach for the removal of retrochiasmatic craniopharyngioma with complicated conditions. This is the first study to report surgical outcomes of the transpetrosal approach for retrochiasmatic craniopharyngioma.

Methods

Indications for MAPC Transpetrosal Approach

Minimum anterior and posterior combined (MAPC) transpetrosal approaches were applied to retrochiasmatic craniopharyngiomas with complicated conditions such as a history of excisions or radiotherapy, tumors with large calcification, large diameter (> 30 mm), superior extension into the third ventricle, or severe posterior extension compressing the midbrain and pons. If a retrochiasmatic craniopharyngioma possessed not less than 2 of these complicated conditions and no well-developed middle fossa venous sinus (such as the sphenobasal or sphenopetrosal sinus) blocking the surgical route to the tumor, the MAPC transpetrosal approach was applied.

Patient Population

Between 1999 and 2011, a total of 44 consecutive patients underwent resection of craniopharyngiomas in the Department of Neurosurgery at Osaka City University in Osaka, Japan. Medical records from all 44 patients were retrospectively examined. Tumors showing the following conditions on imaging were defined as retrochiasmatic craniopharyngiomas: 1) the tumor extending toward the posterior fossa and upward toward the third ventricle, displacing the midbrain posteriorly and the optic chiasm anteriorly; and 2) no upward displacement of the anterior cerebral arteries as would be seen in patients with a prechiasmatic craniopharyngioma. Thirty-six of the 44 tumors were classified as retrochiasmatic craniopharyngioma and 16 of these 36 tumors were resected using our modified MAPC transpetrosal approach. These 16 cases formed the sample for this study. All clinical data of the 16 patients were reviewed retrospectively.

Six patients were male and 10 patients were female, and their mean age at the time of surgery was 47.9 years (range 27–71 years; Table 1). Eight patients (50.0%) had undergone previous surgical procedures at other institutions (Table 1). Prior surgical approaches were interhemispheric in 3 patients, pterional in 2, extended transsphenoidal in 2, and orbitozygomatic in 2. Ommaya reservoirs had been placed in 2 patients. Four patients had received repeated or combined operations. The mean interval between first surgery and our surgery was 10.0 years (range 0.7–32.0 years). Four patients had already received radiotherapy prior to referral to our institution. Stereotactic radiosurgery was added in 2 cases, conventional radiotherapy to 1, and conventional radiotherapy and 3 sessions of stereotactic radiosurgery in 1. The mean maximum diameter of the tumor, as estimated from preoperative MR images, was 32.1 mm (range 25–40 mm). A large tumor diameter (maximum tumor diameter > 30 mm) was present in 11 patients (68.8%). A large calcification (intratumoral calcification > 10% of tumor volume on preoperative CT images) was present in 10 patients (62.5%). Superior extension into the third ventricle was documented in 15 patients (93.8%). Posterior extension in which the tumor appeared to be compressing the midbrain and pons was present in 10 patients (62.5%). All 16 patients had no fewer than 2 of these complicated conditions (Table 1).

Nine tumors were removed in a single step via the MAPC transpetrosal approach and 7 tumors were excised in 2 steps via a combination of the MAPC transpetrosal approach and other approaches (for example, orbitozygomatic, interhemispheric lamina terminalis, and transsphenoidal). The mean follow-up duration was 5.3 years (range 0.8–12.5 years). The median survival duration was 5.6 years (range 1.4–12.5 years). Three patients died during the follow-up period: 1 patient of radiation necrosis 3.6 years after surgery; 1 of chronic heart failure 6.1 years after surgery; and 1 of old age 1.7 years after surgery. Another patient was followed up for 0.8 years before being lost to follow-up after being transferred to another hospital for an unrelated disease 1.4 years after surgery. Clinical and ophthalmological examinations, imaging studies, endocrinological studies, neuropsychological function, and surgical complications were reviewed retrospectively based on the medical records at our institution.

Neuroradiological Evaluation

Before surgery, all patients underwent MRI, CT, and angiography. Tumor size was estimated from MR images by measuring the maximum anteroposterior, vertical, and horizontal diameters. The extent of intratumoral calcifica-

TABLE 1: Characteristics of 16 patients with tumors resected via the MAPC transpetrosal approach*

Case No.	Age (yrs), Sex	Previous Op	Interval Btwn Ops (yrs)†	Previous Radiation	Max Tumor Diameter (mm)	Calcification (%)	Superior Extension into 3rd Ventricle	Posterior Extension Compressing Brainstem
1	31, F				25	>50	yes	no
2	63, F	PT × 4	32	conventional RT	32	<10	yes	yes
3	69, F				40	>10	yes	yes
4	27, F	OZ × 2, Ommaya	1.6		27	>10	yes	yes
5	60, F				30	none	yes	no
6	30, M				31	none	yes	no
7	39, M	IH	3.7	SRS	36	none	yes	yes
8	71, F				37	>50	yes	no
9	69, M				36	none	yes	yes
10	45, M				31	<10	yes	yes
11	34, F	OZ, extended TSS	1.2		25	>10	no	no
12	47, M	extended TSS	0.7		38	>10	yes	yes
13	69, F				30	>50	yes	yes
14	33, F	PT × 3, Ommaya × 2	18	SRS × 3, conventional RT	25	>50	yes	no
15	33, M	IH	5.3	SRS	26	>50	yes	yes
16	61, F	IH	18		44	>10	yes	yes

* IH = interhemispheric approach; OZ = orbitozygomatic approach; PT = pterional approach; RT = radiation therapy; SRS = stereotactic radiosurgery; TSS = transsphenoidal surgery.

† Interval between first surgery and surgery at our institution.

tion was determined on CT images. Intratumoral calcification that accounted for more than 10% of the tumor volume was defined as large calcification. Anatomical features of the cerebral vessels, such as the extent of development of the posterior communicating artery (PCoA) and the development of venous drainage on the lesion side, were evaluated on angiograms. Precise understanding of venous flow in the middle and posterior fossa is mandatory to safely complete the transpetrosal approach. For example, the insertion of the petrosal vein into the superior petrosal sinus represents a key landmark for ligation of the superior petrosal sinus and the cerebellar tentorium. In addition, a well-developed sphenobasal sinus without sufficient collateral venous flow represents one of the most significant hazards to the transpetrosal approach. These fine venous findings can currently only be obtained on 3D angiography. We therefore performed angiography in all cases in addition to MR angiography.

Extent of Tumor Resection

Neuroradiologists independently reviewed the results of preoperative and postoperative MR and CT images to assess the extent of tumor resection. The extent of resection was determined from MR and CT images obtained within 1 week after surgery and from follow-up radiological studies. All tumors were evaluated using enhanced MRI. However, small calcifications can only be detected on CT, which is why this modality was used for radiological evaluation. If small calcifications were identified, a small residual tumor was considered to be present. Small enhanced lesions that diminished in the late period were judged as representing postoperative reactive changes rather than as residual tumor.

Resection was classified as gross-total resection when there was no residual enhanced lesion or residual calcification, near-total resection when residual enhanced lesion or calcification was limited to less than 0.5 cm^3, and subtotal resection when there was residual enhanced lesion or calcification was equal to or less than 0.5 cm^3. The volume of the residual enhanced lesion or calcification was calculated as the volume of an ellipsoid: volume = $4\pi abc/3 \times 2^3$, where a, b, and c represent the orthogonal diameters on the MR image.

Tumor Recurrence

Follow-up MRI was performed within 1 week after surgery, within 3 months after surgery, and then at regular intervals of 6–12 months. Three patients underwent the second MRI session at 4 months after surgery rather than within 3 months. All other patients underwent MRI in accordance with the schedule. Recurrence of the tumor during follow-up was defined as the appearance of new pathological tissue on MR images or the growth of tumor remnants.

Visual Function

Ophthalmological evaluation, including visual acuity and field examination in accordance with the guidelines of the German Ophthalmological Society, was performed by an ophthalmologist before and after surgery and when clinically appropriate. The timing of subsequent assess-

ments was decided on an individual basis. Visual function was quantified using the visual impairment scale (VIS), which is based on visual acuity and visual field defects in both eyes (Fig. 1).[7] Available ophthalmological examinations including visual acuity and visual field testing for reviews were performed in 15 cases. One patient who was transferred to another hospital for an unrelated disease during the follow-up period did not undergo full ophthalmological evaluation.

Endocrinological Status

In addition to clinical symptoms, we evaluated basic levels of luteinizing hormone, follicle-stimulating hormone, free triiodothyronine, free thyroxine, thyroid-stimulating hormone, growth hormone, cortisol, adrenocorticotropic hormone, and prolactin before and after surgery. Anterior pituitary hormone dysfunction was defined as the use of hormone supplementation; deficits in basic levels of luteinizing hormone, follicle-stimulating hormone, free triiodothyronine, free thyroxine, thyroid-stimulating hormone, growth hormone, cortisol, or adrenocorticotropic hormone; or high levels of prolactin without use of dopamine agonists. Diabetes insipidus was diagnosed before and after surgery based on sodium level and the presence of hypotonic polyuria. All patients underwent available endocrinological assessment for review.

Neuropsychological Function

Neuropsychological function was evaluated preoperatively and postoperatively by face-to-face examinations. Patients were classified as showing neuropsychological dysfunction if any of the following conditions were met: 1) score < 70 on the full scale of the Wechsler adult intelligence scale (3rd edition);[28] 2) score < 20 on the Mini-Mental Status Examination;[9] or 3) the patient found it impossible to continue in a previous occupation. These data were available for review from all patients.

Functional Performance Status

Functional performance status was evaluated using the Karnofsky Performance Scale (KPS).

Statistical Analysis

The cumulative risk of tumor recurrence was calculated according to the Kaplan-Meier method; JMP 9.0 software (SAS Institute Inc.) was used.

The MAPC Transpetrosal Approach

Positioning. Patients were placed in a semiprone park bench position. The head was fixed using 3-point fixation with the head rotated and vertex down to keep the temporal side of the head in the horizontal plane.

Skin Incision. The skin incision started at the upper margin of the zygomatic arch anterior to the tragus, turned 2–3 cm above the ear, and then descended behind the posterior margin of the mastoid process. After reflecting the skin flap, a temporal fascia-pericranial flap with a pedicle of the sternocleidomastoid muscle was harvested to prevent leakage of CSF.

Craniotomy. Temporo-occipito-suboccipital craniotomy was performed prior to mastoidectomy. Key bur holes were placed at 4 anatomical landmarks to avoid injuring the sigmoid sinus. The first bur hole was made at the asterion, the second at the intersection of the supramastoid crest with the squamous suture, the third at the mastoid emissary foramen, and the fourth just at the inion-asterion line. The first bur hole was usually just above the lateral end of the transverse sinus, the second just anterior to the transverse-sigmoid sinus junction, the third a few millimeters medial to the posterior edge of the sigmoid sinus, and the fourth just on the transverse sinus.

Preparation for MAPC Petrosectomy. After temporo-occipito-suboccipital craniotomy, the outer cortical bone of the mastoid portion of the temporal bone was removed as a thin triangular plate for cosmetic mastoidectomy. This procedure was not essential and was skipped in cases in which the groove of the sigmoid sinus was too large. At this point, the transverse sinus and transverse sinus–sigmoid sinus junction had been safely exposed (Fig. 2A). Dural dissection from the petrous and mastoid portions of the temporal bone was then started for safe and swift petrosectomy. At the middle fossa, the dura matter at the temporal base was gently reflected to fully expose the entire course of the petrous ridge and apex by cutting the middle meningeal artery and dissecting the greater superficial petrosal nerve. At the posterior fossa, the presigmoid dura was carefully dissected from the posterior surface of the petrous portion of the temporal bone and the entrance of the internal auditory canal was epidurally exposed by cutting the endolymphatic sac (Fig. 2B). After completion of this dural dissection, bone work for petrosectomy was performed (Fig. 2C). This full dural retraction is a unique characteristic of the MAPC transpetrosal approach. The membranous labyrinths of the semicircular canals were kept intact to preserve hearing. A small amount of bone at the petrous ridge was drilled out to obtain a surgical corridor along the axis of the petrous ridge (Fig. 2D and E). The amount of petrous portion of the temporal bone required for petrosectomy is quite limited and this allows a quick surgical procedure.

Dural Opening. The presigmoid dura was opened along the drilled petrosal portion of the temporal bone as far anteriorly as possible while the insertion of the petrosal vein at the superior petrosal sinus was inspected. The subtemporal dura was opened anteriorly and the superior petrosal sinus was divided by Weck clips (Teleflex) at a point anterior to the insertion of the petrosal vein at the superior petrosal sinus to preserve venous reflux from the petrosal vein. The tentorium was cut behind the dural entrance of the trochlear nerve, and the trochlear nerve into the tentorium was exposed.

Intradural Procedure. After superior retraction of the temporal lobe and medial mobilization of the sigmoid sinus, the arachnoid membrane was dissected to obtain a surgical corridor to the retrochiasmatic space (Fig. 3A). The trochlear nerve, oculomotor nerve, C_1 and C_2 portions of the internal carotid artery, PCoA and its perforating branches, posterior cerebral artery, and superior cerebellar artery were identified step by step; the tumor was widely

Visual acuity

L \ R	1,0	0,8	0,63	0,5	0,4	0,32	0,25	0,2	0,16	0,1	0,08	0,05	0,02	0
	5/5	5/6	5/8	5/10	5/12	5/15	5/20	5/25	5/30	5/50	1/12	1/20	1/50	0
1,00 5/5	0	2	4	6	8	10	12	15	17	20	22	25	27	30
0,8 5/6	2	4	8	10	12	15	17	20	22	25	27	30	32	35
0,63 5/8	4	8	15	17	20	22	25	27	30	32	35	37	40	42
0,5 5/10	6	10	17	20	22	25	27	30	32	35	40	42	45	47
0,4 5/12	**8**	**12**	**20**	**22**	**25**	**30**	**32**	**35**	37	40	42	47	50	52
0,32 5/15	10	15	22	25	30	35	40	45	47	50	55	57	60	62
0,25 5/20	12	17	25	27	32	40	50	52	55	57	60	65	67	70
0,2 5/25	15	20	27	30	35	45	52	55	57	60	65	70	75	80
0,16 5/30	17	22	30	32	37	47	55	57	60	65	70	75	80	85
0,1 5/50	20	25	32	35	40	50	57	60	65	75	80	85	87	90
0,08 1/12	22	27	35	40	42	55	60	65	70	80	85	90	92	95
0,05 1/20	25	30	37	42	47	57	65	70	75	85	90	98	100	100
0,02 1/50	28	32	40	45	50	60	67	75	80	87	92	100	100	100
0 0	30	35	42	47	52	62	70	80	85	90	95	100	100	100

Visual field defect

L \ R												
	0	2	4	5	5	5	5	5	5	5	5	0
	2	6	8	8	10	14	18	19	20	25	2	
	4	8	10	12	14	16	20	21	22	27	4	
	5	8	12	14	16	18	22	22	23	28	6	
	5	10	14	16	18	20	22	23	24	29	8	
	5	14	16	18	20	**22**	24	25	26	31	10	
	5	18	20	22	22	24	26	28	35	40	15	
	5	19	21	22	23	25	28	30	40	45	20	
	5	20	22	23	24	26	35	40	45	48	25	
	5	25	27	28	29	31	40	45	48	50	25	
	0	2	4	6	8	10	15	20	25	25	0	

Fig. 1. Tables of visual acuity and visual field defects used to calculate the VIS score. The *black boxes with numbers* provide an example of the calculation made in a patient with a visual acuity of 0.4 in the left eye and 0.2 in the right eye, together with a bitemporal visual field defect. The VIS score is the sum of these 2 numbers (that is, 35 + 22 = 57). Reprinted with permission from Fahlbusch R, Schott W: *J Neurosurg* 96:235–243, 2002.

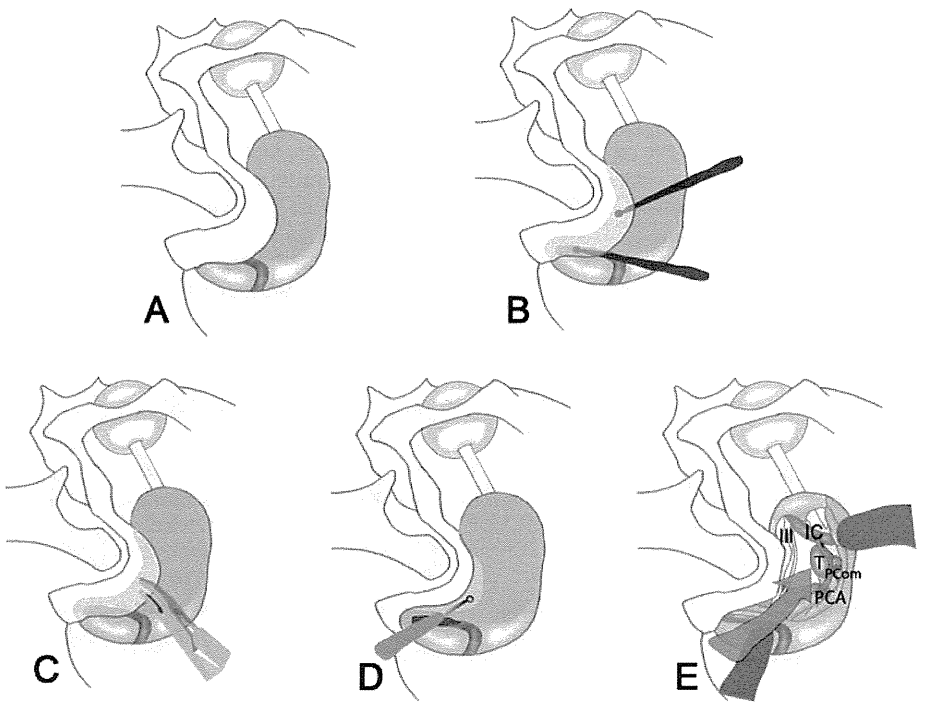

Fig. 2. Illustrations of petrosectomy used in the MAPC transpetrosal approach. **A:** The transverse sinus and transverse sinus–sigmoid sinus junction are safely exposed after temporo-occipito-suboccipital craniotomy and cosmetic mastoidectomy. **B:** Dural dissection from the petrous and mastoid portions of the temporal bone is completely performed at the middle fossa and the posterior fossa. **C:** Complete exposed petrous portion of temporal bone is safely and quickly removed in the wide surgical field. **D:** A small amount of bone at the petrous ridge is drilled out to create a unique surgical corridor. **E:** The wide exposure and unique posterior-to-anterior and inferior-to-superior projection for retrochiasmatic craniopharyngiomas are offered by the MAPC transpetrosal approach *(red arrow)*. IC = internal carotid artery; PCA = posterior cerebral artery; PCom = PCoA; T = tumor; III = third cranial nerve. Copyright Noritsugu Kunihiro. Published with permission.

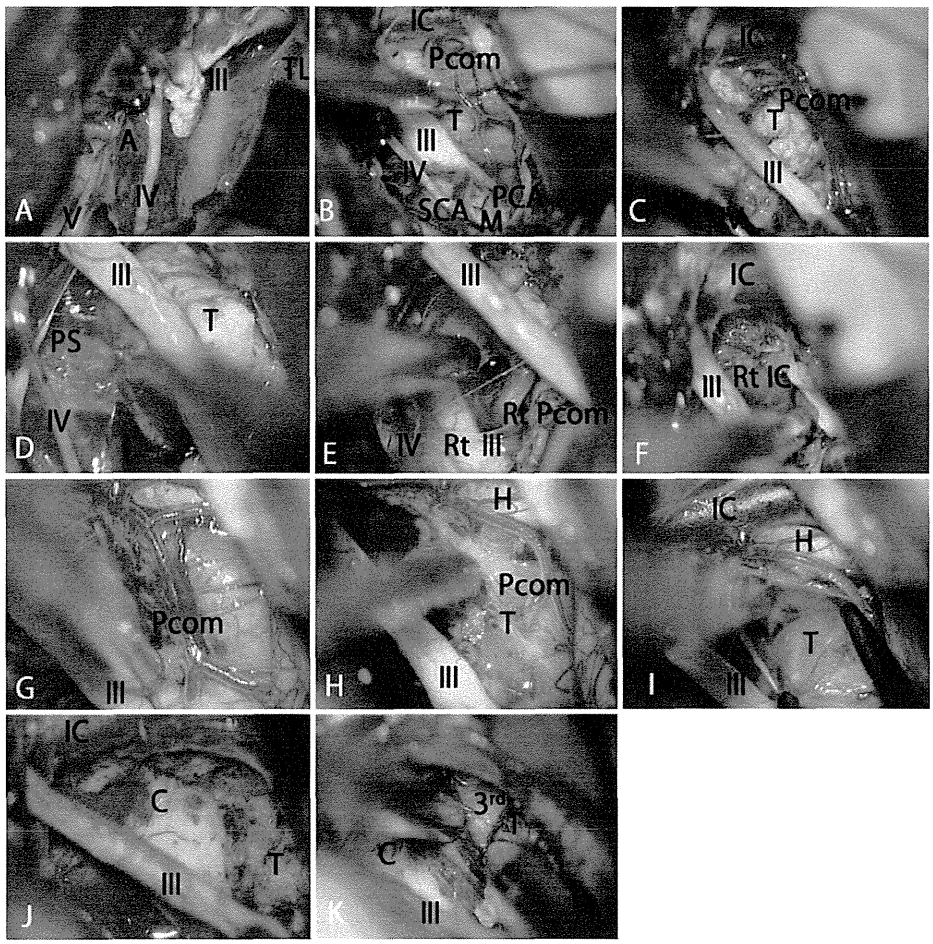

Fig. 3. Intraoperative photographs of intradural exposure and tumor removal achieved using the MAPC transpetrosal approach. **A:** Initial exposure of the vital retrochiasmatic space reveals cranial nerves covered with arachnoid membrane (A). **B:** The corridor of the MAPC transpetrosal approach is widely exposed to reveal the tumor (T) and vital neurovascular structures near the tumor. **C:** The space between the oculomotor nerve (III) and PCoA (Pcom) as well as below the oculomotor nerve provides wide surgical fields for tumor resection. **D:** The pituitary stalk (PS) is well visualized through the space below the oculomotor nerve. **E and F:** The right oculomotor nerve (Rt III), the right PCoA (Rt Pcom), and the right internal carotid artery (Rt IC) are well visualized. This allows preservation of perforating arteries from the PCoA. **G and H:** The upward mobilization that follows the division of the PCoA; the mobilization offers wider operative space and wide exposure of the tumor around the inferior surface of the hypothalamus (H). **I:** The direct visualization of the change in appearance of tissue between the tumor and hypothalamus provides a safe gliotic plane of dissection. **J:** The inferior and posterior surface of the chiasm (C) is well visualized via posterior-to-anterior and inferior upward projection. **K:** The medial wall of the third ventricle (3rd) is well visualized after more upward projection. IV = fourth cranial nerve; M = midbrain; PCA = posterior cerebral artery; SCA = superior cerebellar artery. TL = temporal lobe; V = fifth cranial nerve.

exposed behind the optic chiasm, under the hypothalamus, and in front of the midbrain (Fig. 3B). In this approach, the space between the oculomotor nerve and PCoA, as well as below the oculomotor nerve, provided useful surgical fields for tumor resection. After the initial internal decompression of the tumor (Fig. 3C), the pituitary stalk was visualized (Fig. 3D) but not often preserved. The inferior portion of the tumor on the contralateral side was dissected from the contralateral oculomotor nerve, PCoA, and internal carotid artery (Fig. 3E and F). The main corridor between the oculomotor nerve and PCoA allowed safe dissection from the surrounding structures, such as the surface behind the chiasm or hypothalamus on direct visualization. The hypoplastic PCoA was often divided at the intersection point with the posterior cerebral artery, and upward mobilization of the PCoA enlarged the operative space (Fig. 3G and H). By obtaining more upward projection through this wider operative space, the tumor was safely dissected off the inferior surface of the hypothalamus (Fig. 3I). As dissection progressed anteriorly, the inferior and posterior surfaces of the chiasm were visualized directly via posterior-to-anterior and inferior-to-superior projection (Fig. 3J). In cases where the tumor extended into posterior fossa, it was dissected away from the basilar artery or lower cranial nerves. The intraventricular part of the tumor with superior extension was dissected from the medial wall of the third ventricle under direct visualization through the more upward projection (Fig. 3K).

Closure. All opened mastoid air cells were sealed with abdominal fat-soaked fibrin glue; then the mastoid and petrous portions of the temporal bone and dural defect were entirely covered with the harvested fascia-pericranial flap. The lumbar drain was left open for approximately 3 days to allow CSF pressure to reduce and prevent leakage of CSF.

Results

Extent of Tumor Resection

The extent of tumor resection is shown in Table 2. Gross-total resection was achieved in 9 patients (56.3%) and near-total resection was achieved in 6 patients (37.5%). Subtotal resection was found in only 1 patient (Case 2). This patient had particularly complicated conditions, including 4 previous surgeries and a history of conventional radiation therapy.

Tumor Recurrence

During the follow-up period, no tumor recurrence occurred in any of the 9 patients with gross-total resection (Table 2). Regrowth was detected in 1 of the 6 patients with near-total resection but was successfully controlled for 108 months after an additional resection and stereotactic radiosurgery. Regrowth began 8 months after surgery in the patient with subtotal resection. This was controlled by additional resection and stereotactic radiosurgery treatment, but the patient died due to radiation necrosis.

Morbidity and Mortality

No surgery-related deaths occurred. Transient oculomotor nerve palsy was confirmed in 7 patients and was fully resolved within the follow-up period. Facial nerve function was completely maintained in all 16 patients. Serviceable hearing was preserved in 15 of the 16 patients. No other cranial nerve palsies were seen. Venous infarction or contusion-related temporal retraction was not detected. Leakage of CSF and surgical-site infection did not occur in any patients (Table 2).

Visual Function

Results of the VIS are presented in Table 2. Fifteen patients (93.8%) showed visual disturbance before surgery. One patient who was lost to follow-up after admission to another hospital with an unrelated disease did not undergo a full ophthalmological evaluation and thus was not included in this analysis. One patient with normal visual function preoperatively retained normal function postoperatively. Visual function improved after surgery in 13 (92.9%) of the 14 patients who had visual disturbance before surgery. One patient (Case 2) did not show improvement in visual function after surgery. This patient was blind in both eyes (VIS score of 100) before surgery. No patients experienced any deterioration in visual function. The mean VIS score improved from 37.2 ± 33.7 preoperatively to 17.3 ± 31.3 postoperatively.

Endocrinological Status

Twelve patients (75.0%) had an endocrinological deficit or had received hormonal replacement before our surgery. Preoperatively, 4 patients had received replacement of anterior pituitary hormone, 6 patients showed a deficit in anterior pituitary hormone, and 9 patients had diabetes insipidus. Three patients showed deficit of anterior pituitary hormone without diabetes insipidus and 2 patients showed only diabetes insipidus. Postoperatively, 14 patients (87.5%) received endocrine replacement (Table 2). Of these patients, 2 received replacement of anterior pituitary hormone without diabetes insipidus and 1 had diabetes insipidus only. Pituitary stalks were anatomically preserved in 6 patients but preservation of function was only achieved in 2 patients.

Neuropsychological Function

Five patients (31.3%) showed neuropsychological deficit before surgery, and the neuropsychological function in the remaining 11 patients (68.8%) was normal. During follow-up, neuropsychological function was preserved in 14 patients (87.5%), improved in 1 patient (6.3%), and deteriorated in 1 patient (6.3%) (Table 2). The patient who had deteriorated neuropsychological function had received previous conventional radiotherapy and showed a gradual decline in neuropsychological function.

Functional Performance Status

Postoperative KPS scores at final follow-up were compared with preoperative KPS scores in 13 patients. Two patients died of unrelated diseases, and 1 patient was lost to follow-up after admission to another hospital with an unrelated disease and thus was not included in this analysis (Table 2). The mean preoperative KPS score was 80.0 (range 60.0–90.0) and the mean postoperative KPS score was 88.3 (range 70.0–90.0). The KPS scores improved in all but 1 patient (Case 2), who died due to radiation necrosis. All patients (except the one who died due to radiation necrosis) returned to their normal daily life and social activities after surgery.

Long-Term Outcome

The recurrence-free survival rate is shown in Fig. 4. The 5-year recurrence-free survival rate in the 16 patients was 86.5% (Fig. 4). The 10-year recurrence-free survival rate was also 86.5% (Fig. 4). The 5-year recurrence-free survival rates were 100.0% after gross-total resection and 68.5% after near-total and subtotal resection (Fig. 5).

Discussion

Craniopharyngiomas located in the retrochiasmatic region are regarded as challenging tumors to remove safely and totally because of their anatomical location and proximity to critical neurovascular structures. Because of the hidden position of retrochiasmatic craniopharyngiomas behind the optic chiasm, their upward extension into the third ventricle, and their downward extension in front of the brainstem, the surgical exposure of these tumors is usually unsatisfactory.[2,20,25,29] Resection of this type of craniopharyngioma has thus been associated with a high rate of surgical mortality, surgical complications, and in-

TABLE 2: Surgical outcomes in 16 patients with tumors resected via the MAPC transpetrosal approach*

					VIS Score						Endocrinological Dysfunction				Neuropsychological Deficit		KPS Score	
					Preop			Postop			Preop		Postop					
Case No.	Approach	Resection	Complication	Recurrence	VA	VF	Total	VA	VF	Total	APH	DI	APH	DI	Preop	Postop	Preop	Postop
1	OZ→TP	GTR	none	no	0	0	0	0	0	0	no	no	no	yes	no	no	90	90
2	TP	STR	none	yes	100	25	100	100	0	100	yes	no	yes	no	no	yes	60	dead†
3	TP	GTR	none	no	28	31	59	2	10	12	no	yes	yes	yes	yes	no	70	dead‡
4	TP→OZ	NTR	none	yes	15	22	37	0	0	0	yes	yes	yes	no	no	no	80	90
5	TP→TSS	GTR	hearing disturbance	no	10	0	10	0	0	0	no	yes	yes	yes	no	no	60	dead‡
6	TP	GTR	none	no	10	10	20	0	0	0	no	no	yes	yes	no	no	80	90
7	TP	NTR	none	no	8	22	30	0	0	0	yes	yes	yes	yes	no	no	80	90
8	TP	GTR	none	no	22	6	28	17	6	23	yes	yes	yes	yes	no	no	80	90
9	TP	NTR	none	no	4	14	18	0	4	4	yes	no	no	no	no	no	80	90
10	TP→OZ	GTR	none	no	20	14	34	0	0	0	yes	yes	yes	yes	yes	yes	80	90
11	TP	NTR	none	no	2	0	2	0	0	0	no	no	no	no	no	no	80	90
12	TP	GTR	none	no	2	22	24	0	22	22	yes	yes	yes	yes	no	no	90	90
13	TP	NTR	none	no	75	22	97		—		yes	no	yes	yes	yes	yes	70	unknown§
14	TP→OZ	NTR	none	no	100	25	100	60	22	82	yes	yes	yes	yes	yes	yes	60	70
15	TP→IH	GTR	none	no	0	18	18	0	0	0	yes	yes	yes	yes	no	no	90	90
16	TP→OZ	GTR	none	no	4	14	18	0	16	16	no	no	yes	yes	yes	yes	90	90

* APH = anterior pituitary hormone; DI = diabetes insipidus; GTR = gross-total resection; NTR = near-total resection; STR = subtotal resection; TP = transpetrosal approach; VA = visual acuity; VF = visual field

† Patient died of radiation necrosis related to the treatment.

‡ Patient died of an unrelated disease.

§ Patient was lost to follow-up.

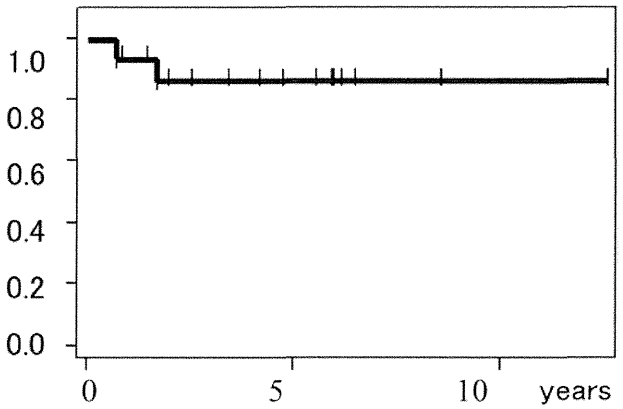

FIG. 4. Recurrence-free survival time (calculated using the Kaplan-Meier method) in patients who underwent surgery for retrochiasmatic craniopharyngiomas via the MAPC transpetrosal approach.

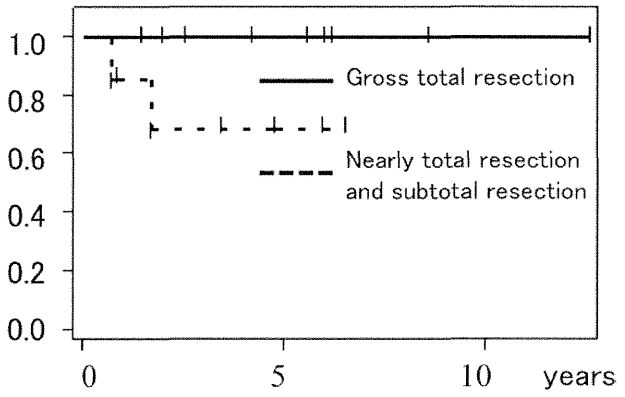

FIG. 5. Recurrence-free survival times (calculated using the Kaplan-Meier method) in relation to the extent of resection in patients who underwent surgery for retrochiasmatic craniopharyngiomas.

complete resection resulting in higher recurrence rates.[6,26] In addition, previous large series of craniopharyngiomas have reported that retrochiasmatic location, larger size, greater than 10% calcification, extension into the third ventricle, and recurrence are significant prognostic factors that negatively affect the extent of resection.[4,6,12,19,21,26,29] Fahlbusch et al. achieved complete resection in only 21.4% of tumors with greater than 10% intratumoral calcification.[6] Several studies have reported that the rate of total resection in repeat surgery is markedly lower than in primary surgery; moreover, perioperative morbidity and mortality are also increased in cases of repeat surgery.[6,12,18,19,26,29] In tumors with posterior extension where the tumor appears to compress the midbrain and pons, most surgeons might recognize that preservation of the membrane of Lilliquist prevents the tumor from adhering to vessels and the brainstem in this area. However, this is less true for recurrent cases. We therefore regarded posterior extension as one of the complicating conditions.

The 16 cases of retrochiasmatic craniopharyngiomas with complicated conditions reported in this series all possessed at least 2 of these risk factors and thus can be regarded as the most challenging subgroup of craniopharyngiomas. Even under such difficult conditions, the results of our MAPC transpetrosal approach were satisfactory in terms of the extent of tumor removal, tumor control, and complication rate. The unique posterior-to-anterior and inferior-to-superior surgical corridor to the retrochiasmatic area afforded by the MAPC transpetrosal approach provides a relatively wide space for surgical procedures in the retrochiasmatic space and offers direct visualization of the posterior and inferior surfaces of the chiasm, the floor of the third ventricle, and the hypothalamic tuber cinereum area. In addition, this posterior-anterior corridor to the chiasm and the third ventricle has the advantage of preserving small perforating vessels from the internal carotid arteries that provide the primary blood supply to the optic chiasm and hypothalamus. These characteristics are distinct from other conventional surgical approaches, such as pterional, orbitozygomatic, and interhemispheric lamina terminalis approaches, and are the primary reason for our good results regarding the extent of tumor removal and preservation of visual function in retrochiasmatic craniopharyngiomas with complicated conditions. The endonasal endoscopic approach can also offer a direct view of the posterior and inferior surfaces of the chiasm, but it is not effective in cases of recurrent tumors, tumors with large calcification, and large tumors because the maneuverability of surgical instruments is not as good as it is when using a microscope, particularly when bipolar forceps are needed for dissection of perforating vessels.[13,16] The endonasal endoscopic approach would thus be unsuitable for the complicated cases reported here.

Despite the effectiveness of the MAPC transpetrosal approach, some considered it to be a time-consuming and difficult procedure that carries a risk of damaging cranial nerves, such as the facial and acoustic nerves, and causing leakage of CSF and surgical-site infection. At our institute, we modified the original transpetrosal approach of Hakuba et al.[11] to overcome these problems and developed the MAPC transpetrosal approach in 1999. In our procedure the dura mater at the middle and posterior fossa is completely peeled off the superior and posterior surfaces of the petrous portion of the temporal bone before the petrosectomy is initiated. This differs from other petrosal approaches and effectively shortens the surgical time for petrosectomy and reduces the extent of bone removal required. For epidural retraction of the temporal and presigmoid dura, a small amount of petrous drilling along the petrous ridge is sufficient to obtain the surgical corridor to the retrochiasmatic space and is also effective in preserving facial and cochlear functions. In fact, hearing was preserved in 15 of the 16 cases and facial function was preserved in all 16 cases. In addition, no surgical-site infection and no leakage of CSF were seen in any of the 16 cases.

A disadvantage of our MAPC transpetrosal approach was an occasional occurrence of transient oculomotor nerve palsy just after the surgical procedure, but we consider this an acceptable complication considering the surgical difficulty of the cases. Seven patients underwent 2-staged operations involving the transpetrosal approach and another approach. One of the reasons for a second operation was that in cases with adhesions between the tu-

mor and the perforator of the opposite internal carotid artery, these parts of the tumor are more difficult to remove safely via the transpetrosal approach. However, these parts could be removed safely using an orbitozygomatic approach from the contralateral side. Another reason is that the part of the sella turcica or the superoposterior part of the third ventricle is more difficult to access directly because the transpetrosal approach provides inferior-to-superior and posterior-to-anterior projections. However, the residual tumors in the sella turcica could be removed safely via transsphenoidal surgery and residual tumors in the superoposterior part of the third ventricle could be removed using an interhemispheric approach.

There is a school of thought that retrochiasmatic craniopharyngiomas with complicated conditions should be treated conservatively with a combination of safe partial resection and stereotactic radiosurgery to reduce the risks of surgery. This conservative treatment has provided acceptable results for some types of craniopharyngiomas.[14,24,25,27] However, of the cases presented in this report, radiotherapies or radiosurgeries had already been applied in 4 cases; radiotherapies or stereotactic radiosurgeries were not acceptable in the other 12 cases because of the proximity of the tumors to the optic chiasm and hypothalamus. In general, radiosurgery is contraindicated if the distance between the tumor and optic apparatus is less than 3 mm because the visual pathways would typically receive more than 10 Gy in these situations.[14] The 16 cases of retrochiasmatic craniopharyngiomas presented in this report could be considered the most difficult cases to control, and radical resection of the tumor should be regarded as the last treatment. Our results regarding extent of tumor removal, tumor control, complication rate, and visual function were satisfactory compared with the other reports of craniopharyngiomas.[4,6,12,19,21,26,29]

Conclusions

Although this represents the first report on surgical outcomes of the transpetrosal approach for retrochiasmatic craniopharyngiomas, we achieved satisfactory results using the MAPC transpetrosal approach for the removal of retrochiasmatic craniopharyngiomas under complicated conditions. The MAPC transpetrosal approach can provide an alternative procedure for resection of retrochiasmatic craniopharyngiomas with complicated conditions such as recurrence, history of radiation, large calcification, large tumor diameter, and extreme superior and posterior extension.

Disclosure

The authors report no conflict of interest concerning the materials or methods used in this study or the findings specified in this paper.

Author contributions to the study and manuscript preparation include the following. Conception and design: Kunihiro, Goto, Ohata. Acquisition of data: Kunihiro, Goto, Ishibashi. Analysis and interpretation of data: Kunihiro. Drafting the article: Kunihiro. Critically revising the article: Goto.

References

1. Al-Mefty O, Ayoubi S, Kadri PA: The petrosal approach for the total removal of giant retrochiasmatic craniopharyngiomas in children. **J Neurosurg 106 (2 Suppl):**87–92, 2007
2. Ammirati M, Samii M, Sephernia A: Surgery of large retrochiasmatic craniopharyngiomas in children. **Childs Nerv Syst 6:**13–17, 1990
3. Dehdashti AR, de Tribolet N: Frontobasal interhemispheric trans-lamina terminalis approach for suprasellar lesions. **Neurosurgery 56 (2 Suppl):**418–424, 2005
4. Duff J, Meyer FB, Ilstrup DM, Laws ER Jr, Schleck CD, Scheithauer BW: Long-term outcomes for surgically resected craniopharyngiomas. **Neurosurgery 46:**291–305, 2000
5. Fahlbusch R, Hofmann BM: Surgical management of giant craniopharyngiomas. **Acta Neurochir (Wien) 150:**1213–1226, 2008
6. Fahlbusch R, Honegger J, Paulus W, Huk W, Buchfelder M: Surgical treatment of craniopharyngiomas: experience with 168 patients. **J Neurosurg 90:**237–250, 1999
7. Fahlbusch R, Schott W: Pterional surgery of meningiomas of the tuberculum sellae and planum sphenoidale: surgical results with special consideration of ophthalmological and endocrinological outcomes. **J Neurosurg 96:**235–243, 2002
8. Fatemi N, Dusick JR, de Paiva Neto MA, Malkasian D, Kelly DF: Endonasal versus supraorbital keyhole removal of craniopharyngiomas and tuberculum sellae meningiomas. **Neurosurgery 64 (5 Suppl 2):**269–286, 2009
9. Folstein MF, Folstein SE, McHugh PR: "Mini-mental state". A practical method for grading the cognitive state of patients for the clinician. **J Psychiatr Res 12:**189–198, 1975
10. Golshani KJ, Lalwani K, Delashaw JB Jr, Selden NR: Modified orbitozygomatic craniotomy for craniopharyngioma resection in children. Clinical article. **J Neurosurg Pediatr 4:**345–352, 2009
11. Hakuba A, Nishimura S, Inoue Y: Transpetrosal-transtentorial approach and its application in the therapy of retrochiasmatic craniopharyngiomas. **Surg Neurol 24:**405–415, 1985
12. Karavitaki N, Brufani C, Warner JT, Adams CBT, Richards P, Ansorge O, et al: Craniopharyngiomas in children and adults: systematic analysis of 121 cases with long-term follow-up. **Clin Endocrinol (Oxf) 62:**397–409, 2005
13. Kim EH, Ahn JY, Kim SH: Technique and outcome of endoscopy-assisted microscopic extended transsphenoidal surgery for suprasellar craniopharyngiomas. Clincal article. **J Neurosurg 114:**1338–1349, 2011
14. Lee M, Kalani MY, Cheshier S, Gibbs IC, Adler JR, Chang SD: Radiation therapy and CyberKnife radiosurgery in the management of craniopharyngiomas. **Neurosurg Focus 24(5):**E4, 2008
15. Liu JK, Christiano LD, Gupta G, Carmel PW: Surgical nuances for removal of retrochiasmatic craniopharyngiomas via the transbasal subfrontal translamina terminalis approach. **Neurosurg Focus 28(4):**E6, 2010
16. Liu JK, Christiano LD, Patel SK, Eloy JA: Surgical nuances for removal of retrochiasmatic craniopharyngioma via the endoscopic endonasal extended transsphenoidal transplanum transtuberculum approach. **Neurosurg Focus 30(4):**E14, 2011
17. Maira G, Anile C, Colosimo C, Cabezas D: Craniopharyngiomas of the third ventricle: trans-lamina terminalis approach. **Neurosurgery 47:**857–865, 2000
18. Minamida Y, Mikami T, Hashi K, Houkin K: Surgical management of the recurrence and regrowth of craniopharyngiomas. **J Neurosurg 103:**224–232, 2005
19. Mortini P, Losa M, Pozzobon G, Barzaghi R, Riva M, Acerno S, et al: Neurosurgical treatment of craniopharyngioma in adults and children: early and long-term results in a large case series. Clinical article. **J Neurosurg 114:**1350–1359, 2011
20. Rutka JT: Editorial. Craniopharyngioma. **J Neurosurg 97:**1–2, 2002
21. Shi XE, Wu B, Fan T, Zhou ZQ, Zhang YL: Craniopharyngioma: surgical experience of 309 cases in China. **Clin Neurol Neurosurg 110:**151–159, 2008

22. Shibuya M, Takayasu M, Suzuki Y, Saito K, Sugita K: Bifrontal basal interhemispheric approach to craniopharyngioma resection with or without division of the anterior communicating artery. **J Neurosurg 84:**951–956, 1996
23. Shirane R, Ching-Chan S, Kusaka Y, Jokura H, Yoshimoto T: Surgical outcomes in 31 patients with craniopharyngiomas extending outside the suprasellar cistern: an evaluation of the frontobasal interhemispheric approach. **J Neurosurg 96:**704–712, 2002
24. Smee RI, Williams JR, Kwok B, Teo C, Stening W: Modern radiotherapy approaches in the management of craniopharyngiomas. **J Clin Neurosci 18:**613–617, 2011
25. Stripp DC, Maity A, Janss AJ, Belasco JB, Tochner ZA, Goldwein JW, et al: Surgery with or without radiation therapy in the management of craniopharyngiomas in children and young adults. **Int J Radiat Oncol Biol Phys 58:**714–720, 2004
26. Van Effenterre R, Boch AL: Craniopharyngioma in adults and children: a study of 122 surgical cases. **J Neurosurg 97:**3–11, 2002
27. Veeravagu A, Lee M, Jiang B, Chang SD: The role of radiosurgery in the treatment of craniopharyngiomas. **Neurosurg Focus 28(4):**E11, 2010
28. Wechsler D: WAIS-III: **Administration and Scoring Manual: Wechsler Adult Intelligence Scale, ed 3.** San Antonio, TX: Psychological Corp, 1997
29. Yaşargil MG, Curcic M, Kis M, Siegenthaler G, Teddy PJ, Roth P: Total removal of craniopharyngiomas. Approaches and long-term results in 144 patients. **J Neurosurg 73:**3–11, 1990

Manuscript submitted April 4, 2013.
Accepted October 3, 2013.
Please include this information when citing this paper: published online November 15, 2013; DOI: 10.3171/2013.10.JNS13673.
Address correspondence to: Noritsugu Kunihiro M.D., Department of Neurosurgery, Osaka City University Graduate School of Medicine, 1-4-3 Asahi-machi, Abeno-ku, Osaka 545-8585, Japan. email: nori9216@med.osaka-cu.ac.jp.

Theranostic Protein Targeting ErbB2 for Bioluminescence Imaging and Therapy for Cancer

Xiao-Jian Han[1,3,5], Ling-Fei Sun[1], Yuki Nishiyama[1], Bin Feng[1,6], Hiroyuki Michiue[1], Masaharu Seno[4], Hideki Matsui[1], Kazuhito Tomizawa[2*]

1 Department of Physiology, Okayama University Graduate School of Medicine, Dentistry and Pharmaceutical Sciences, Okayama, Japan, **2** Department of Molecular Physiology, Faculty of Life Sciences, Kumamoto University, Kumamoto, Japan, **3** Japan Society for the Promotion of Science, Tokyo, Japan, **4** Department of Medical and Bioengineering Science, Graduate School of Natural Science and Technology, Okayama University, Okayama, Japan, **5** Institute of Translational Medicine, Nanchang University, Nanchang, China, **6** Department of Biotechnology, Dalian medical University, Dalian, China

Abstract

A combination of molecular-targeted cancer imaging and therapy is an emerging strategy to improve cancer diagnosis and minimize the side effects of conventional treatments. Here, we generated a recombinant protein, EC1-GLuc-p53C, by fusing EC1 peptide, an artificial ligand of ErbB2, with *Gaussia* luciferase (GLuc) and a p53-activating peptide, p53C. EC1-GLuc-p53C was expressed and purified from *E. coli* BL21. *In vitro* experiments showed that EC1-GLuc-p53c was stable in luminescent activity and selectively targeted ErbB2-overexpressing BT474 cells for bioluminescence imaging. Moreover, the internalized EC1-GLuc-p53C in BT474 cells exerted its function to reactivate p53 and significantly inhibited cellular proliferation. In tumor-bearing mice, the ErbB2-targeted bioluminescence imaging and therapeutic effect of EC1-GLuc-p53C were also observed specifically in BT474 tumors but not in MCF7 tumors, which does not overexpress ErbB2. Thus, the present study demonstrates EC1-GLuc-p53C to be an effective theranostic reagent targeting ErbB2 for bioluminescence imaging and cancer therapy.

Citation: Han X-J, Sun L-F, Nishiyama Y, Feng B, Michiue H, et al. (2013) Theranostic Protein Targeting ErbB2 for Bioluminescence Imaging and Therapy for Cancer. PLoS ONE 8(9): e75288. doi:10.1371/journal.pone.0075288

Editor: Xiaoyuan Chen, NIH, United States of America

Received April 18, 2013; **Accepted** August 12, 2013; **Published** September 17, 2013

Funding: This work was supported by grant-in-aid for Young Scientists (B) from the Ministry of Education, Science, Sports and Culture of Japan (No: 21790202,http://www.waseda.jp/rps/en/manual/kakenhi_honbun.html) and by Grant-in-aid for Scientific Research from the Japan Society for the Promotion of Science (No: 22.00119,http://www.jsps.go.jp/english/e-grants/). The funders had no role in study design, data collection and analysis, decision to publish, or preparation of the manuscript.

Competing interests: The authors have declared that no competing interests exist.

* E-mail: tomikt@kumamoto-u.ac.jp

Introduction

ErbB2 is a member of the epidermal growth factor receptor (EGFR) family of receptor tyrosine kinases, also called the ErbB family. The ErbB family includes four members, ErbB1, ErbB2, ErbB3 and ErbB4. There are several endogenous ligands for ErbB receptors with the exception of ErbB2 [1]. The tyrosine kinase activity of ErbBs can be activated by endogenous ligands and the homo- or hetero-dimerization of ErbB receptors, which is involved in the regulation of cellular proliferation and cell survival [1-3]. In addition, ErbB2 has been implicated in tumor pathogenesis and progression [4-6]. Clinically, overexpression of ErbB2 is associated with approximately 30% of breast cancers, ovarian cancers [7] and other common types of cancers including lung, gastric, and oral cancers [8]. The overexpression is also associated with the metastasis, therapeutic resistance and poor prognosis of cancer [9-11]. Thus, ErbB2 may be a promising molecular target for cancer imaging and treatment using monoclonal antibodies and peptide-targeting vectors [12,13]. In a phage display study, several small artificial cyclic peptides with specific affinity for ErbB2 were identified. EC1, one of these artificial peptides, bound the extracellular domain of ErbB2 in living cells and fresh frozen human breast cancer specimens [14]. Moreover, biotin-conjugated EC1 and the recombinant protein EC1-eGFP retained affinity for ErbB2 and were internalized by ErbB2-overexpressing cancer cells [14,15]. Recently, divalent and multivalent forms of EC1-Fc ligand in liposomes were reported to improve affinity for ErbB2 and enhance internalization [16]. Thus, EC1 peptide may be a potential artificial ligand for targeting ErbB2.

In tumor pathogenesis, several abnormal mutations are found in tumor-suppressor genes. One of the best-known tumor-suppressor genes is *p53*, which is an important regulator of apoptosis and the most commonly mutated gene in cancer [17,18]. Restoration of p53 activity has been proved to be an effective means of treating cancer cells with p53 mutations [19,20]. In our previous studies [21-23], a full-length

recombinant p53 was successfully delivered into human malignant glioma cells, oral and bladder cancer cells by fusing with poly-arginine, a cell-penetrating peptide (CPP). It was found that the full-length recombinant p53 had a significant inhibitory effect on the proliferation of cancer cells. However, the large molecular size and rapid degradation by the ubiquitin-proteasome pathway greatly influenced the efficiency of protein transduction and effect of the transduced p53 on cancer cells [24]. The C-terminus of p53 is a lysine-rich domain subject to a variety of posttranslational modifications [25,26]. A peptide derived from the C-terminus activates specific DNA binding with p53 *in vitro* through an unknown mechanism [27]. It was reported that the p53-derived C-terminal peptide (p53C) induced rapid apoptosis in breast cancer cells carrying endogenous p53 mutations or overexpressed wild-type (wt) p53, but was not toxic to nonmalignant human cell lines containing wt p53 [28]. In addition, p53C peptide fused with CPP inhibits the proliferation of cancer cells by reactivating endogenous p53, and significantly increases lifespan in animal models of terminal peritoneal carcinomatosis and bladder cancer *in vivo* [29-31]. These studies demonstrate the reactivation of the p53 protein by p53C peptide to be a promising means for cancer therapy.

Bioluminescence imaging is emerging as a relatively simple, cost-effective and extremely sensitive way to monitor dynamic biological processes in intact cells and living animals [32]. In recent years, the technology has developed rapidly with improvements in luciferase reporters and instrumentation [33]. The most common luciferases for bioluminescence imaging include *Firefly* luciferase (FLuc), *Renilla* luciferase (RLuc) and *Gaussia* luciferase (GLuc). Each luciferase has distinct properties in the application of bioluminescence imaging. FLuc (62 kDa) catalyzes the oxidation of luciferin to yield bioluminescence in the presence of O_2, magnesium and ATP [34]. RLuc (36 kDa) and GLuc (19.9 kDa) catalyze the oxidative decarboxylation of coelenterazine to emit light independent of ATP. However, RLuc has a lower quantum yield than FLuc, and also less enzymatic efficiency [35,36]. GLuc yields approximately 200- (*in vivo*) to 1000-fold (*in vitro*) more bioluminescence in mammalian cells than FLuc and RLuc [37]. Therefore, its small molecular size (19.9kDa), independence from ATP and strong emission make GLuc much more suitable for bioluminescence imaging *in vitro* and *in vivo* [38,39].

The concept of "Theranostic" was originated by Funkhouser in 2002 from one of his reviews [40]. Theranostics is defined as a material that combines the modalities of therapy and diagnostic imaging at the same time within the same dose. The goal of theranostic is to donate materials with the capacity of monitoring the treated tissue and efficacy in the long-term period [41]. Theranostic reagents have been developed fast in the previous decade, especially after the emergence of some new optical probes and potent biomolecules for targeting and therapy. In the present study, a novel ErbB2-targeting bioluminescence protein was constructed by fusing EC1 with GLuc and p53C peptide. Two human breast carcinoma cell lines, MCF7 without expression of ErbB2 and BT474 overexpressing ErbB2, were employed to evaluate the role of EC1-GLuc-p53C in specific bioluminescence imaging and cancer therapy. We observed that EC1-GLuc-p53C not only targeted ErbB2 for bioluminescence imaging, but also selectively inhibited cell proliferation and tumor growth of BT474 *in vitro* and *in vivo*. The present results indicate that EC1-GLuc-p53C may be a promising theranostic reagent targeting ErbB2 for bioluminescence imaging and therapy.

Materials and Methods

Cell culture and detection of ErbB2 expression

The MCF7 and BT474 cell lines were obtained from the American Type Culture Collection (ATCC). BT474 cells carry a missense mutation (E285K) in the p53 gene [42], while MCF7 cells with overexpression of wt p53 [28]. BT474 cells were grown in a RPMI-1640 medium supplemented with 10% fetal bovine serum (FBS) and 100 μg/ml penicillin-streptomycin (P/S). MCF7 cells were cultured in DMED medium supplemented with 10% FBS and 100 μg/ml P/S. The mediums, FBS and P/S were from Invitrogen. All cultures were maintained in a humidified incubator at 37°C with an atmosphere containing 5% CO_2.

The expression of ErbB2 in MCF7 and BT474 cells was examined by Western immunoblotting. Briefly, MCF7 and BT474 cells on 35mm dishes were washed once with PBS, and scraped in 1×SDS sample buffer. Cell lysates were subjected to 6% SDS-PAGE, and immunoblotted with Rabbit anti-ErbB2 antibody (1:1000; Cell Signaling) overnight at 4°C. HRP-conjugated secondary antibody (Sigma-Aldrich) was used at 1:2000. Immunoblotting signals were detected by the Versa Doc 5000 imaging system (Bio-Rad) with an enhanced chemiluminescence detection kit (Amersham Biosciences, Pittsburgh, PA).

Plasmid construction

The pGLuc plasmid was purchased from LUX biotechnology Ltd (Scotland, UK). The GLuc gene was amplified from the plasmid using a sense primer (5'-GGATCCGAAACCAACTGAAAACAATGAAG-3') and antisense primer (5'-GTCGACATCACCACCGGCACCCTTTAT-3'). The PCR product was ligated into the pCR2.1 TOPO vector (Invitrogen) for amplification, and recloned in the pET52b vector (Invitrogen) to construct GLuc-pET52b. The following sense and antisense oligonucleotides (Hokkaido System Science, Japan) with appropriate resistance enzyme sites for EC1 or p53C peptide were prepared; for EC1; 5'-GGGTGGACTGGCTGGTGCCTGAATCCAGAAGAATCTACTT GGGGATTCTGTACTGGATCTTTCGGTGGAGGTAGTTCAG-3' (sense, underline indicates *Sam* I and *Bam*HI sites) and 5'-GATCCTGAACTACCTCCACCGAAAGATCCAGTACAGAATC CCCAAGTAGATTCTTCTGGATTCAGGCACCAGCCAGTCCA CCC-3' (antisense, underline indicates *Bam*HI and *Sam* I sites), and for p53C; 5'-TCGACGGGAGCAGGGCTCACTCCAGCCACCTGAAGTCCA AAAAGGGTCAGTCTACCTCCCGCCATAAAAAAGGCGC-3' (sense, underline indicates *Sal*I and *Not*I sites), and 5'-GGCCGCGCCTTTTTTATGGCGGGAHHTAGACTGACCCTTT TTGGACTTCAGGTGGCTGGAGTGAGCCCTGCTCCCG-3' (sense, underline indicates *Not*I and *Sal*I sites). The

oligonucleotides for EC1 and p53C were modified by phosphorylation at 5'. The sense and antisense oligonucleotides (10 pmol each) were co-incubated at 95°C for 10 min, and annealed at room temperature to form double-stranded DNA. The double-stranded DNA for EC1 or p53C was ligated to GLuc-pET52b treated with the appropriate resistance enzymes to construct EC1-GLuc-pET52b or EC1-GLuc-p53C-pET52b. Site-directed mutagenesis was introduced at BamHI in EC1-GLuc and EC1-GLuc-p53C using a QuikChange kit (Stratagene) according to the manufacturer's instructions. The primers for mutagenesis were 5'-GTGGAGGTAGTTCAGGAACCAAACCAACTG-3' (sense, underline indicates the mutated nucleotide), 5'-CAGTTGGTTTGGTTCCTGAACTACCTCCAC-3' (antisense). GLuc, EC1-GLuc and EC1-GLuc-p53C were then subcloned into pGEX-6p-1 between the *Bam*HI and *Eco*RI sites for protein purification. The sequences of constructed plasmids were confirmed using an ABI 3100 sequencer.

Expression and purification of recombinant proteins

The expression and purification of recombinant proteins were performed as described previously [21]. Briefly, *E. coli* BL21 (DE3) transformed with the plasmid for GLuc, EC1-GLuc or EC1-GLuc-p53C was grown in a LB medium containing 100 μg/mL ampicillin at 37°C. When the OD600 reached 0.6, expression of the GST-fused proteins was induced by adding 0.2 mM isopropyl 1-thio-β-D-galactopyranoside at 25°C overnight. The fusion proteins were purified using a column of glutathione Sepharose 4 Fast Flow (GE Healthcare). To cleave GST from the fusion proteins, the purified proteins were further treated with PreScission protease (GE Healthcare) according to the manufacturer's instructions. Recombinant proteins were subjected to 15% SDS-PAGE, and confirmed by Coomassie brilliant blue staining and immunoblotting with rabbit anti-*Gaussia* Luciferase serum (1:1000, Nanolight). The proteins were finally dialyzed against PBS, and concentrations were determined using a protein assay kit (Bio-Rad Laboratories). Aliquots of protein were stored at -80°C prior to use.

Preparation of coelenterazine (CTZ)

The substrate for GLuc was prepared as described previously [32]. Briefly, CTZ (Nanolight) was dissolved in acidified methanol (1 drop of concentrated HCl (12.4 N) in 10 mL of methanol) to a concentration of 5mg/ml. Aliquots of 100μl were stored at -80°C. For luminescence imaging, the aliquots of CTZ (5mg/mL) were diluted with PBS (containing 5mM NaCl, pH 7.2) for higher light output and more stability.

Assays of the luminescent activity and stability of recombinant proteins

To determine the luminescent activity of the purified proteins, 2μg of each protein was transferred to a 96-well plate. Bioluminescence was measured using a plate luminometer (Microlumat plus LB 96V, Berthold technologies) after the addition of 10 μl of CTZ (20 μM). Bioluminescent activity was reported in relative light units (RLU) measured with a 10 sec integration time and calculated as RLU per micromole for each protein. The values for EC1-GLuc and EC1-GLuc-p53C were normalized with GLuc.

The stability of recombinant proteins was assessed as described previously [38]. Aliquots of protein were incubated with an equal volume of mouse serum (Sigma) at 37°C. At each time point, samples were withdrawn for bioluminescence imaging and Western blotting. In the analysis of bioluminescence stability, the percentage of the initial amount of RLU at each time point was plotted for each protein. To detect the degradation of proteins after the incubation with serum, samples withdrawn at each time point were subjected to electrophoresis in 15% acrylamide SDS-PAGE gel, and immunoblotted with rabbit anti-*Gaussia* Luciferase serum at a dilution of 1:1000. HRP-conjugated secondary antibody (Rabbit; Sigma-Aldrich) was used at 1:2000.

Bioluminescence imaging *in vitro*, Internalization by ErbB2-overexpressing cells and WST-1 assay

For bioluminescence imaging *in vitro*, MCF7 and BT474 cells were cultured on 35-mm glass-bottomed dishes. To improve the adherence of MCF7 and BT474 cells, all glass-bottomed dishes were pre-coated with laminin (Roche). MCF7 and BT474 cells were incubated with 1μM of each protein for 24h. After three washes with DMEM, bioluminescence was detected with an Olympus Luminoview LV 200 (Bio-luminescence microscope) immediately after the addition of 1 μg/mL CTZ in serum-free DMEM. Images were acquired and analyzed with Metamorph software (Molecular devices).

To examine the internalization of EC1-fused proteins in ErbB2 overexpressing cancer cells, BT474 cells were incubated with 1 μM of GLuc, EC1-GLuc or EC1-GLuc-p53C. In blocking study, BT474 cells were treated with anti-ErbB2 antibody against extra-cellular domain of ErbB2 (Chicken, 1.0 μg/mL, abcam) 1 h prior to incubation with EC1-GLuc or EC1-GLuc-p53C. After 24 h, cells were washed with PBS three times and trypsinized. Cell lysate was prepared and subjected to 15% SDS-PAGE. The internalization of fusion protein was immunoblotted with rabbit anti-*Gaussia* Luciferase serum. β-actin was used as an endogenous control.

To evaluate the therapeutic effect of EC1-GLuc-p53C *in vitro*, cell viability was determined using a WST-1 assay as described previously [21]. After 3.0×10^3 MCF7 and 1.0×10^4 BT474 cells were seeded on 96-well flat-bottomed plates, they were cultured in DMEM or RPMI1640 medium containing 10% fetal bovine serum for 24 h. The cells were then supplemented with 1μM of protein or PBS (day0) and further cultured 96 h (day4). Cell viability from day 0 to day 4 was measured using the WST-1 assay according to the manufacturer's instructions (Roche Applied Science). To determine the dose-dependent effect of EC1-GLuc-p53C on the proliferation of BT474 cells, the protein was used at 0.1 ~ 2.0 μM, and the WST-1 assay was conducted on day 4.

Reporter Assay for p53-driven Transactivation

The reporter assay was performed as described previously [22]. Briefly, the luciferase reporter vector pGL2-basic (Promega) containing a 2.4 kbp fragment of the human $p21^{WAF1}$ promoter was a gift from Drs. T. Akiyama (Tokyo University)

and K. Yoshikawa (Osaka University). BT474 cells grown until 80% confluent in 35 mm-diameter dishes were transfected with the luciferase reporter vector by lipofectamine 2000 (Invitrogen). After 24 h, the cells were incubated with 1μM of GLuc, EC1-GLuc, EC1-GLuc-p53C or the same volume of PBS for 24h, and further cultured in new medium 2 h prior to cell harvest. The cell lysate was used for measuring luciferase activity with a luminometer and Luciferase Assay System (Promega). The background luciferase activity was subtracted in all experiments. Five independent experiments were performed for each condition.

Preparation of tumor-bearing mice

Nude mice (Balb/c Slc-nu/nu, female, 6~8 weeks) were purchased from Charlesriver, Japan. The plan of animal experiments was reviewed and approved by the ethics committee for animal experiments of Okayama University under the IDs OKU-2010378, OKU-2011400. 17β-estradiol pellets (0.72 mg; Innovative Research of America) were implanted 4 days before tumor cell transplantation and remained in place until the end of the study. The cultured MCF7 and BT474 cells were washed twice with PBS, typsinized, and harvested by centrifuge. Cells (5.0×10^6 cell) suspended in Matrigel (BD Bioscience) were transplanted subcutaneously on both flanks of anesthetized mice with intraperitoneally injection of 5mg/100g pentobarbital solution under aseptic conditions. Mice with tumors developed for 10~14 days were used for *in vivo* experiments. During tumor development, breath and behavioral activity were monitored twice every day to evaluate pain in mice. Experiments were immediately stopped if mice appeared significant symptom of pain. All mice were sacrificed by intraperitoneally injection of 15mg/100g pentobarbital solution after experiments.

The expression of ErbB2 in MCF7 and BT474 xenografts was confirmed by immunofluorescence (IF) staining. Paraffin-embedded slices of tumors were prepared at a thickness of 5 μm. First, histological observations of xenografted tumors were made using H&E staining. IF staining was then performed with anti-ErbB2 antibody (1:50; Cell Signaling). The secondary antibody was Cy3-conjugated anti-rabbit IgG (1:100; Invitrogen, Molecular probes). The nucleus was counter-stained with 0.1 μg/ml of Hoechst 33248 (Sigma) for 5 min. Fluorescence signals were observed using a confocal laser microscope (FV300, Olympus).

Tumor site retention of EC1-GLuc-p53C in tumor xenografts

Next, 30 μL of EC1-GLuc-p53C protein (0.5 μg/μL) was injected intratumorally into MCF7 and BT474 xenografts in nude mice. At 1, 3, 6, 12 and 24 hours after the injection, the mice were sacrificed. Tumors were excised and immediately fixed with 4% paraformaldehyde. Paraffin-embedded slices of MCF7 and BT474 tumors were prepared at 10 μm. Immunofluorescence staining was carried out to analyze the distribution of EC1-GLuc-p53C in tumors. The immunofluorescence staining was performed according to the instructions that accompanied the rabbit anti-*Gaussia* Luciferase serum. The secondary antibody was FITC-conjugated rabbit IgG (1:100, Invitrogen, Molecular probes). Fluorescence signals were observed using a confocal laser microscope (FluoView, Olympus, Japan).

Bioluminescence imaging *in vivo*

For bioluminescence imaging *in vivo*, 30 μl of EC1-GLuc-p53C protein (0.5 μg/μl) was intratumorally injected into the MCF7 and BT474 xenografts established in nude mice. At 6, 8, 12 and 24 hours after the injection, mice were imaged by injection via a tail vein with 100 μl of CTZ solution (3 mg/Kg) under anesthesia using a cooled CCD camera (IVIS Lumina-II, Caliper Life Sciences) as described previously [39]. The bioluminescent intensity of the selected region over the tumor was recorded as maximum photons s^{-1} cm^{-2} $steradian^{-1}$.

Effect of EC1-GLuc-p53C on tumor growth

MCF7 and BT474 xenografts on both flanks of nude mice were allowed to grow until an average volume of ~ $100mm^3$ ± $10mm^3$ was obtained prior to protein injection. Then, 30 μL of purified recombinant protein (0.5 μg/μL) or 30 μL of PBS was intratumorally injected into MCF7 and BT474 xenografts everyday for 5 days. The mice were monitored daily and their tumor volume was measured using digital vernier calipers twice week. During the whole course of therapy in tumor burden experiment no mouse died. Tumor volume was calculated according to the formula: tumor volume=$L\times W^2\times0.5$ (L is the longest diameter, W is the shortest diameter).

Statistical analysis

Data are shown as the mean±SD or mean±S.E.M. Data were analyzed using either Student's t test to compare two conditions or ANOVA followed by planned comparisons of multiple conditions, and $P<0.05$ was considered to be significant.

Results

Purification and biochemical characterization of the recombinant proteins

The three GST-fused protein constructs were expressed in *E. coli* BL21 and purified using a column of glutathione Sepharose 4 Fast Flow. After purification, the GST tag was cleaved by PreScission protease to harvest GLuc, EC1-GLuc and EC1-GLuc-p53C as shown in Figure 1a. GLuc and EC1-GLuc were used as control proteins. Coomassie brilliant blue staining revealed the purity of all three proteins to be > 80%. The molecular sizes of GLuc, EC1-GLuc and EC1-GLuc-p53C were approximately 20, 23, and 25KDa, respectively (Figure 1b). In Western blotting, the main bands of GLuc, EC1-GLuc and EC1-GLuc-p53C and additional minor bands corresponding to the GST-fused proteins were observed (Figure 1c). Moreover, a loss in bioluminescent activity was induced by the fusion of EC1 and p53C peptide with GLuc. An approximately 30% and 50% reduction was detected in the bioluminescent activity of EC1-GLuc and EC1-GLuc-p53C compared with GLuc, respectively (Figure 1d).